Ocean Engineering 255 (2022) 111445

Contents lists available at ScienceDirect

Ocean Engineering

journal homepage: www.elsevier.com/locate/oceaneng

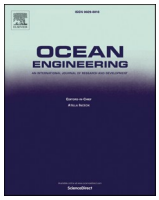

Experimental study on the effect of biomimetic tubercles on the drag of a flat plate

Roberto Ravenna [a,*], Alessandro Marino [a], Soonseok Song [b], Mehmet Atlar [a], Osman Turan [a], Sandy Day [a], Yigit Kemal Demirel [a]

[a] University of Strathclyde, Department of Naval Architecture, Ocean and Marine Engineering, UK
[b] Inha University, South Korea

ARTICLE INFO

Keywords:
3D printed biomimetic tubercles
Flat plate towing tank tests
Resistance coefficients
Experimental fluid dynamics (EFD)

ABSTRACT

The necessity to improve the hydrodynamic performance of marine vessels has confirmed the urgency of conducting further investigations on biomimetic tubercles. In this work, towing tank tests were conducted at a range of speeds on conveniently prepared flat plates coated with 3D printed humpback whales mimicked tubercles.

The results showed that the artificial tubercles induced a drag reduction of up to 1.3% compared to the bare flat plate. Following the experimental campaign presented, some relevant considerations for ship owners and naval architects will be proposed.

1. Introduction

Although shipping is considered more environmentally friendly than other forms of transportation (e.g. aviation and land), it is responsible for 2.8% of the total CO_2 emissions a year (IMO, 2015). The International Towing Tank Conference (ITTC) considerably recommends that researchers develop new methods to improve the efficiency of ship resistance (ITTC, 2017a).

"Biomimetics" is the transfer of ideas and analogues from biology to technology (Vincent et al., 2006). The goal of this novel approach is to engineer systems that emulate the mechanisms of living systems or their constructs, particularly in instances in which an organism's performance exceeds current human-engineered technologies (Taubes, 2000; Mohseni et al., 2006; Fish, 2009). Biomimetic tubercles represent particular warty round outgrowths exhibited by multiple organisms such as Humpback whales (*Megaptera Novaengliae*), (Fig. 1). Tubercles are reported on the leading-edge of the pectoral fins and the head of humpback whales during scientific observations (Clapham and Mead, 1999; Clapham, 2018). According to the literature, the tubercles on the pectoral fins enhance the fluid flow behaviour over the flipper's surface, exhibiting the so-called *tubercle effect* of fluid dynamics (Fish and Lauder, 2006; Fish et al., 2011). Moreover, they enhance the manoeuvrability of humpback whales, which are incredibly agile mammals capable of quick movements and underwater acrobatics. Thus, humpback whales are seen in this study as templates for performance-enhancing solutions.

The function of the tubercles of the head of humpback whales is not fully-understood; scientists suggested that it could be sensorial too (Mercado, 2014; Clapham, 2018). Tubercles could have a tactile function as their inner structure is highly innervated, as Pacinian corpuscles in terrestrial mammals (Mercado, 2014). Marino et al. (2019) conducted a CFD study on the effect of head tubercles on a flat plate.

Extensive research has been carried out for the leading-edge biomimetic tubercles on flat plates, foils and wing profiles, (Miklosovic et al., 2004; Hasheminejad et al., 2013; Shi et al., 2015; Bolzon et al., 2016). The marine application of leading-edge tubercles focuses on rudders (Weber et al., 2009) and tidal turbines (Shi et al., 2016a; Shi et al., 2016b; Gruber et al., 2011).

The aeronautical application of leading-edge tubercles on foils and wings, discussed in (Fish et al., 2011), represents the more significant part, e.g., wind tunnel studies of leading-edge sinusoidal tubercles on flat plates as in (Dobre et al., 2006). These protuberances positively influence the overall performance of these objects, despite a possible slight drag increase due to more energy exchange with the fluid. Although the phenomena that occur to the flow are uncertain, all the authors agree that the possible reason for the benefits produced can be found in the impact of the tubercles on the wake decay or lift and drag fluctuations (Bolzon et al., 2016). Bugatti car manufacturer recently patented a new design utilising the tubercle effect for enhanced aerodynamics. They mounted morphing shape tubercles on top of the

* Corresponding author.
E-mail address: roberto.ravenna@strath.ac.uk (R. Ravenna).

https://doi.org/10.1016/j.oceaneng.2022.111445
Received 15 July 2021; Received in revised form 22 January 2022; Accepted 28 April 2022
Available online 9 May 2022

Fig. 1. Tubercles on the head and pectoral fins of a humpback whale/Flickr NOAA Photo Library/https://flickr.com/photos/51647007@N08/9614765647.

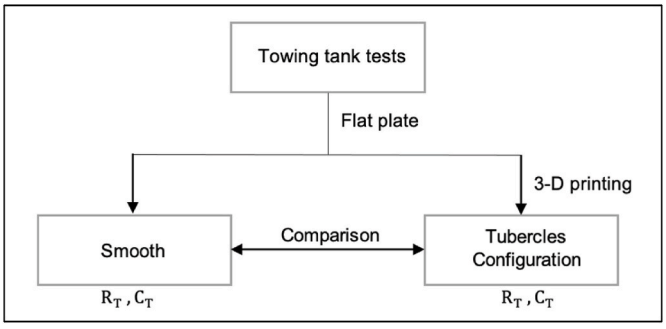

Fig. 2. Schematic of the methodology adopted.

air-intake scoop of their newest hyper-car *Bolide*, actively manipulating the laminar flow at certain speeds ("Bugatti Dimple Airscoop," 2020).

All the studies mentioned above acknowledge that the tubercles produce streamwise contra-rotating vortices, altering the boundary layer and the flow direction within.

The application of leading-edge and trailing edge tubercles on wing profiles has demonstrated the benefits in terms of drag reduction (Fish et al., 2011).

To the authors' best knowledge, no experimental study investigates the effects of "head" tubercles on the hydrodynamics of a marine structure, either a simple submerged flat plate or a ship hull. Therefore, this study aims to conduct an experimental investigation on the effect of biomimetic tubercles on the hydrodynamics of a flat plate.

Towing tank tests were conducted with 3-D printed artificial tubercles on flat plates in smooth conditions and with different tubercles configurations. The total resistance coefficients for the given configurations were determined from the towed plate tests and then compared to the total resistance of the bare flat plate. The aim of this research is to explore the possibility of improving the hydrodynamic efficiency of the hull employing humpback whale-like tubercles.

The structure of this paper is as follows: in the Methodology section is discussed the experimental approach adopted in this study, including the mathematical formulations for drag and total resistance coefficients of flat plates and the setting-up of tubercles for towing tests. The test results for the different configurations of tubercles tested compared with the bare flat plate results and Uncertainty Analysis are presented in the following section. The last part of this study covers the Conclusions and future recommendations.

Fig. 3. Towing carriage of KHL.

2. Methodology

The towing tank tests were carried out at the Kelvin Hydrodynamics Laboratory (KHL) of the University of Strathclyde (UK) following the state-of-the-art procedures suggested by the International Towing Tank Committee (ITTC, 2011). The towing tank tests carried out can be distinguished in smooth flat plate tests (bare flat plate with no tubercles) and tubercles configurations test (Fig. 2). A consistent procedure has been adopted to evaluate the hydrodynamic resistance coefficients of the different scenarios. The results of the total resistance coefficient components were then compared and discussed.

According to Froude, the total resistance of a flat plate can be decomposed into two main components: the frictional resistance R_F and the residuary resistance R_R, as given in equation (1):

$$R_T = R_F + R_R \tag{1}$$

The frictional resistance occurs due to shear stresses on the plate's surface. Given that the pressure resistance component is negligible for thin bodies (Lewis, 1988), the residuary resistance arises due to the wave-making resistance and the separation at the trailing edge of the flat plate. The values of the total resistance measured were non-dimensionalised to obtain the total resistance coefficient C_T, as follows in equation (2):

$$C_T = \frac{R_T}{\left(\frac{1}{2}\,\rho\, S\, V^2\right)} \tag{2}$$

where: ρ is the water density; S is the wetted surface of the flat plate (S does not include the negligible added surface of the tubercles as it is 0.035% of S); C_T is the total resistance coefficient; V is the towing speed.

The preparation of the flat plate models and the towing tests were carried at KHL towing tank. The tank is 76.0 m long, 4.6 m wide and 2.5 m deep, and it is equipped with a digitally controlled towing carriage, a state-of-the-art absorbing wavemaker, and a highly effective sloping beach. The carriage (Fig. 3) velocity ranges from 0 to 5 m/s, but the velocity range used in these experiments was kept between 1.5 and 4.5 m/s. Due to the limit of the towing carriage, the highest speed was 4.5 m/s which is fast enough for standard model tests. The minimum speed could not be lower than 1.5 m/s because of the high uncertainties that

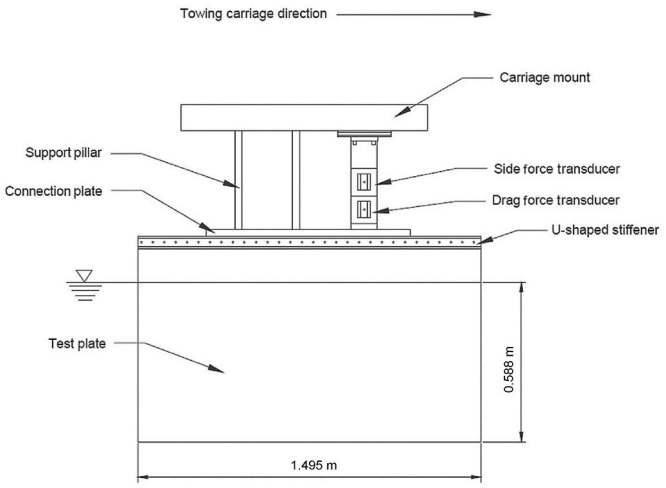

Fig. 4. Schematic of the test set up.

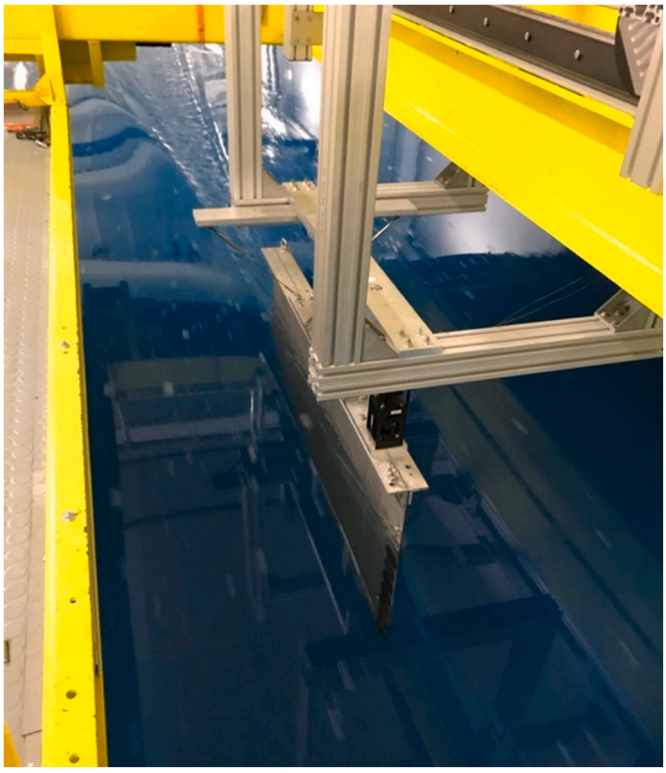

Fig. 5. Flat plate with Upstream rows of tubercles towed at 4.5 m/s.

would have arisen. The freshwater temperature has been monitored throughout the towing tests.

Fig. 4 presents the schematic of the test set-up, which is similar to that of Demirel et al. (2017) and Song et al. (2021). Two displacement transducers were interposed between the test plate and the carriage (Fig. 4) to measure the towed plate's drag and side force. The single-component force sensor transducers were separately calibrated following the procedure of (ITTC, 2002), (ITTC, 2017b). These instruments from Cambridge Electronic Design use the Linear Variable Differential Transformer (LVDT) principle. During the towing tests, the two transducers measured the towed plate's drag force and side force, respectively.

The test flat plate (304 stainless steel) thickness was 5 mm, and its other dimensions are given in Fig. 4. The leading-edge and trailing-edge

Table 1
Details of tubercles on the head of a calf humpback whale.

Tubercle dimensions	Humpback whale calf	Biomimetic model
Height [mm]	7–25	10
Basal diameter [mm]	57–120	74

of the flat plate were milled. In particular, the leading edge was rounded with a radius of 2.5 mm, while the trailing edge was kept flat sharp. The whole plate was scrubbed with acetone solvent to eliminate impurities. All these steps were done to reduce the bare flat plate's undesired extra drag force and side force.

Once the plate was installed on the rig of the carriage, repeated runs were conducted to find the correct alignment. The repeated tests were performed to estimate the uncertainty for the drag coefficients at the lowest and highest speeds of the range (1.5 and 4.5 m/s, respectively). The uncertainty estimate procedure adopted (ITTC, 2002), (ITTC, 2017b) and (Coleman and Steele, 1999), was similar to the one used for the present calibration of instruments mentioned above. The results of the uncertainty analysis can be found in Section 3.1. below.

2.1. Tests

The plate was towed longitudinally (Fig. 5) at a range of speeds for each configuration, and the drag force was measured. The range of speed tested was 1.5–4.5 m/s, with an increment of 0.2 m/s. A minimum of two repeats at the lowest and highest speeds of the range was carried out for repeatability and uncertainty analysis. The total resistance coefficients were obtained from equation (2).

2.2. Geometry model

The geometry model of the biomimetic tubercles tested (Fig. 7) was chosen according to Marino et al. (2019). This model resembled the anatomical size and shape of scientists' findings described in (Mercado, 2014) for the tubercle of the head of humpback whale calves (Table 1).

The model was axisymmetric and presented a basal circumference whose thickness was kept to the minimum printable of 0.1 mm. The sinusoidal defining the top boundaries has a wavelength of 74 mm and a height of 10 mm. The diameter of 74 mm allows covering the draft of the plate with seven tubercles. Because of the space constraints on the flat plate, the number of tubercles per row was such that the whole depth was covered. The number of tubercles per row of the present configurations is seven for the *Upstream, Mid-length and Downstream* configurations Fig. 8. The distributed configuration counts eleven tubercles spatially distributed to mimic their natural distribution on the head of humpback whales. On the other hand, in Marino et al. (2019), the number of tubercles per row is ten, and the flat plate in the CFD model is fully submerged (Fig. 6).

The tubercle model was implemented using the CAD software Rhinoceros in order to be successfully 3-D printed. The presence of stagnation points was checked to obtain the best quality of printings. The biomimetic tubercles were 3-D printed using an Ultimaker printer. Each tubercle was hand smoothened using sandpaper of 400 grit to enrich the surface finish, as recommended by ITTC (ITTC, 2017a). Double-sided tape was chosen as a reliable, cost-efficient, rapid solution to stick the tubercles onto the flat plate easily, with particular attention to the need to assemble the different configurations between test sessions quickly.

The area of the tubercles in the three single-row configurations was designed to be symmetric with respect to the longitudinal midline of the wetted surface of the plate. Similarly, the tubercles area of the *Distributed* configuration was centred in the wetted surface of each side of the plate. The configurations of tubercles adopted for the flat plate were four, as listed below and shown in Fig. 8.

It should be noted that the pictures in Fig. 8 show the plates clamped upside down on a support. After preparing the configurations, these test

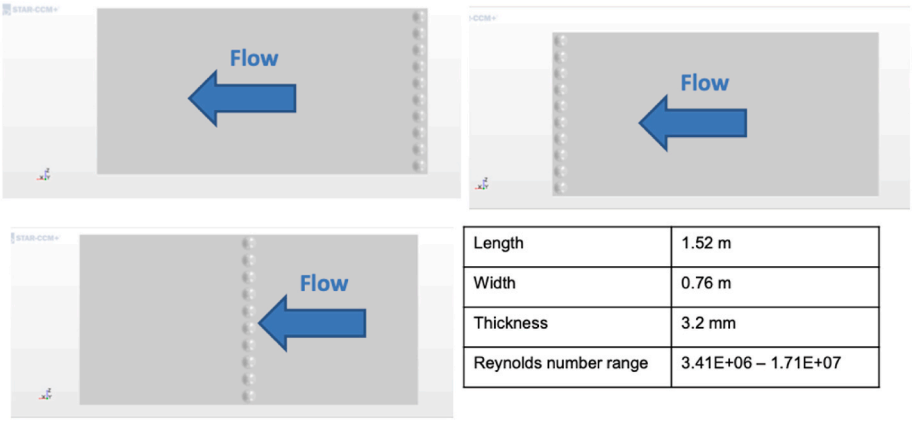

Length	1.52 m
Width	0.76 m
Thickness	3.2 mm
Reynolds number range	3.41E+06 – 1.71E+07

Fig. 6. CFD test configurations, Marino et al. (2019).

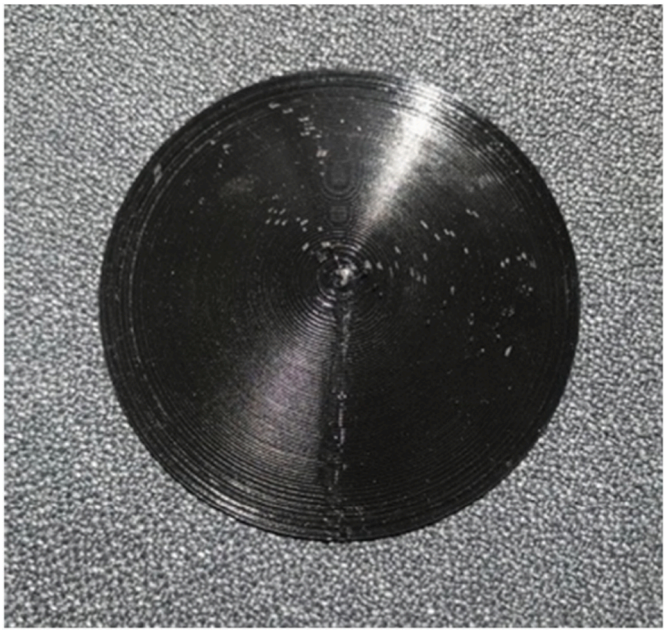

Fig. 7. 3D printed tubercle before being smoothened.

plates were rotated and rigged to the carriage, facing up the rigging area. These experimental tests were similar to the CFD simulations performed by Marino et al. (2019).

The findings of Marino et al. (2019) suggested that the most significant drag reduction across the scenarios mentioned above is given by the *Midlength* configuration, followed by the *Upstream* one. In their simulations, the *Downstream* configuration shown an opposite effect, increasing the drag of the flat plate. In the present study, as will be shown in the next paragraph, only the *Upstream* and *Downstream* scenarios gave drag reductions. Another difference between the CFD study of Marino et al. (2019) and the present experimental campaign is that the *Distributed* configuration has been tested only experimentally. To give an insight into the flow mechanism behind the tubercle effect, Fig. 9 shows the velocity profiles around the row of tubercles.

In the present study, each side of the plate in the *Distributed* configuration counts 11 tubercles equally spaced on the wetted area. Both sides of the plate were fitted symmetrically with the same number and position of tubercles. This configuration can be seen as a simplified representation of the actual upside part of the head of a typical humpback whale calf. It was in the authors' intention to understand how *Distributed* tubercles would change the hydrodynamics of a flat plate. Specular rows of seven tubercles were positioned at the *Upstream* edge, at *Mid-length*, and at the *Downstream* edge.

3. Results and discussion

3.1. Total resistance coefficients

In Fig. 10, the total resistance coefficients, C_T, obtained from equation (2) are plotted against the Reynolds numbers, *Rn*.

All the C_T trendlines plotted in Fig. 8 are polynomials of the 4th order. The good fit of the regression lines was guaranteed by checking that the R-Squared values were close to unitary for all of the data sets. All of these curves present a decreasing trend at increasing *Rn*.

The highest and lowest values of C_T characterise the *Upstream* configuration. Therefore, the *Upstream* configuration of tubercles shows the steepest decrease of all the configurations. Comparing this scenario of tubercles with the bare flat plate, it can be noted that at *Rn* lower than $3.02{\cdot}10^6$, the drag increase is consistent (up to 14.12% at the lowest speed of the range). On the other hand, when the test speed is between $3.02{\cdot}10^6$ and $4.07{\cdot}10^6$, there is a transitional behaviour of the tubercle effect from a negative to a positive influence on resistance. A consistent drag reduction effect was measured for the Upstream configuration at *Rn* higher than $4.07{\cdot}10^6$ up to the upper limit of the range.

In other words, the presence of the row of tubercles *Upstream* of the flat plate gives an appreciable drag reduction. The findings are highlighted in Fig. 8, where it can be seen that the C_T curve for the *Upstream* configuration lays under the *Reference* curve of the smooth plate. The C_T curve of the *Reference* plate shows a flat behaviour at high *Rn* which is similar to the *Upstream* configuration. Thus, the comparison between the two configurations is most evident. Similar behaviour of the *Upstream* case is found for the *Downstream* configuration.

Only the total resistance coefficients values have been presented because directly related to the total drag measured during the experiments. According to Froude, (Lewis, 1988), the residuary resistance could be considered constant across the flat plate configurations. Therefore, the frictional resistance coefficients C_F would simply be shifted below the total resistance coefficients C_T of the residuary resistance coefficients C_R values. In other words, the trend of the total resistance coefficients would be the same of that of the frictional resistance coefficients. Thus, neither the C_F nor C_R values are presented in this study.

Table 2 presents a comparison between the drag and the C_T experimental data at 15 °C for the smooth *Reference* plate and the tubercles configurations. The values corresponding to the *Upstream* and *Downstream* rows of tubercles represent the beneficial reductions obtained. These values are highlighted in green (Tables 2 and 3).

The trend of the total resistance coefficient curve of the Upstream

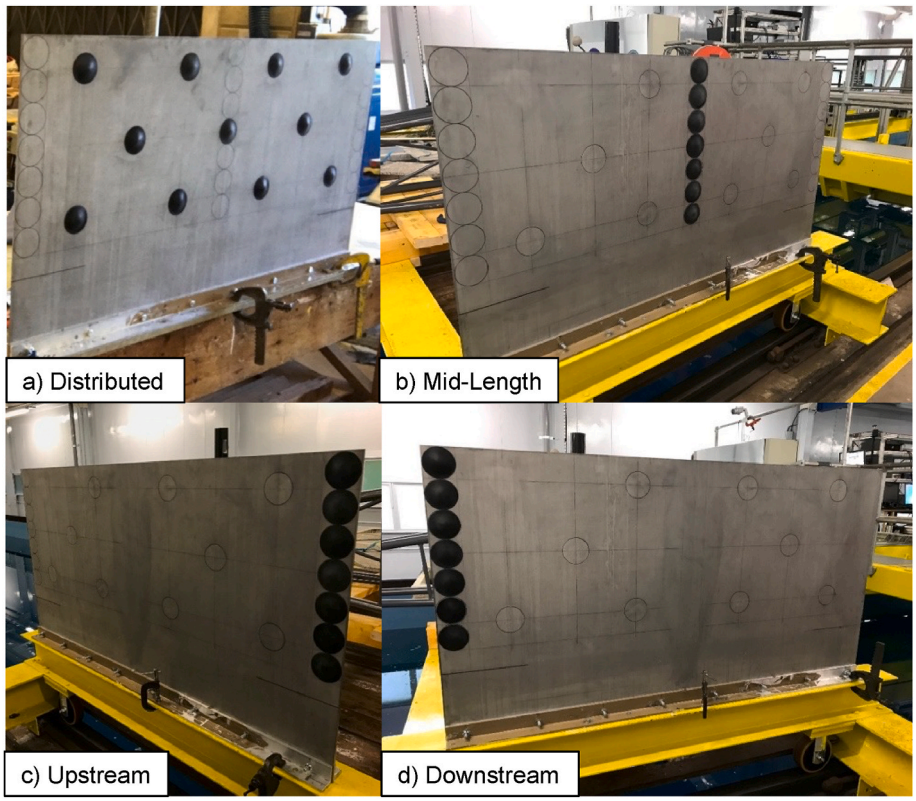

Fig. 8. Tubercles Configurations tested.

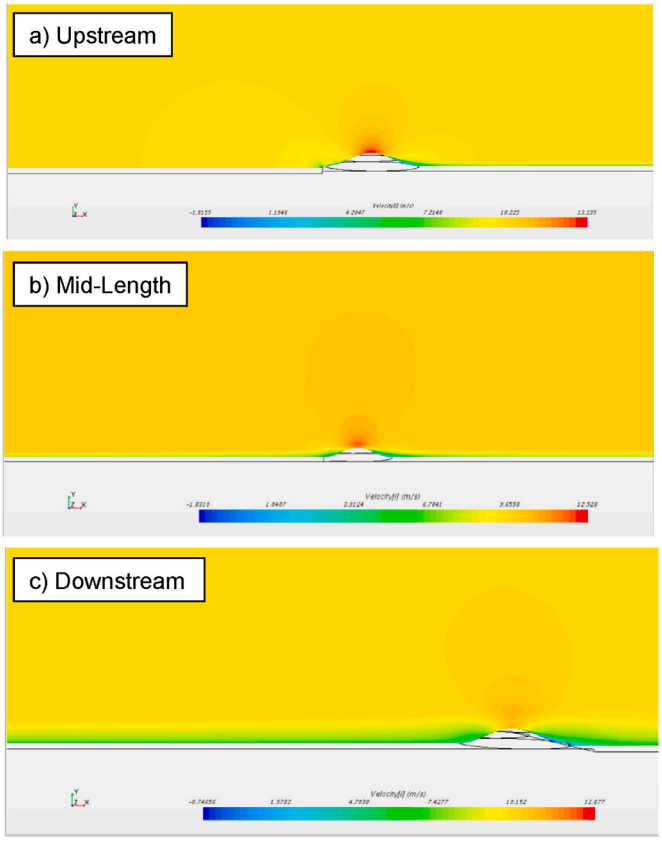

Fig. 9. Velocity profiles around the row of tubercles, Marino et al. (2019).

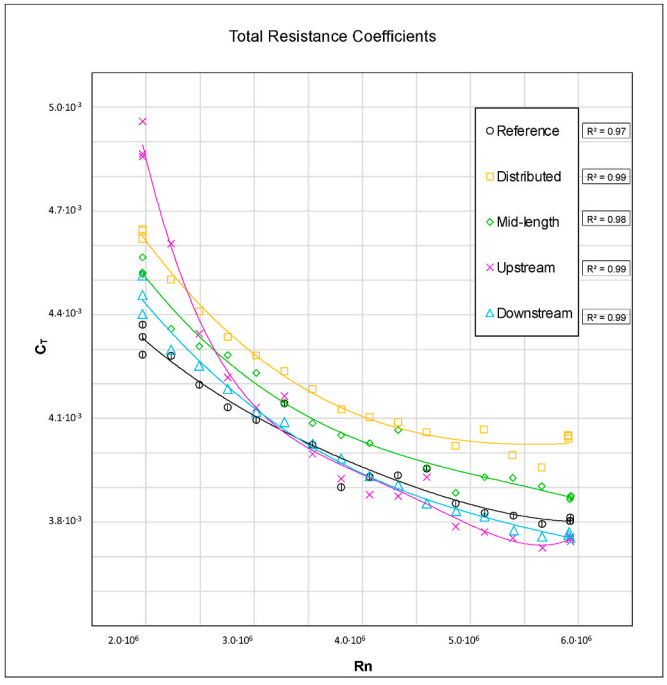

Fig. 10. Experimental results: C_T curves for the whole range of Rn tested.

configuration of tubercles in Fig. 8 is neatly showing the benefits in terms of resistance at high speeds. The values of C_T for the Upstream at high speeds are up to 1.84% less than those of the Reference plate. The values in red in Tables 2 and 3 underline degraded performances for the Distributed and Mid-length configurations. As expected, the Distributed configuration presents an increase of drag for the whole range of speed.

Table 2
– Experimental Data at 15°C for velocities between 1.5 and 2.9 m/s: variation of R_T and C_T with respect to the Reference plate.

Reference	$V\ [m/s]$	1.5	1.7	1.9	2.1	2.3	2.5	2.7	2.9
	Rn	$1.97\ 10^6$	2.2310^6	2.4910^6	2.7610^6	3.0210^6	3.2810^6	3.5410^6	3.8110^6
	$R_T\ [N]$	8.48	10.85	13.27	15.97	19.00	22.69	25.71	28.79
	C_T	4.28410^{-3}	4.28110^{-3}	4.19710^{-3}	4.13210^{-3}	4.09610^{-3}	4.14310^{-3}	4.02410^{-3}	3.90110^{-3}
Distributed	ΔR_T %	9.84	6.91	6.85	6.66	6.25	3.88	5.66	7.42
	ΔC_T %	8.37	5.13	5.06	4.93	4.54	2.25	4.01	5.74
Midlenght	ΔR_T %	5.93	2.65	3.53	4.48	4.11	0.74	2.31	4.60
	ΔC_T %	6.01	2.72	3.54	4.53	4.16	0.79	2.37	4.67
Upstream	ΔR_T %	14.12	8.46	4.37	2.90	1.66	1.25	0.11	1.36
	ΔC_T %	13.57	7.58	3.51	2.07	0.87	0.51	−0.68	0.61
Downstream	ΔR_T %	3.25	1.22	2.16	2.09	1.37	−0.57	0.81	2.87
	ΔC_T %	2.74	0.42	1.30	1.29	0.58	−1.29	0.06	2.11

Table 3
Experimental Data at 15°C for velocities between 3.1 and 4.5 m/s: variation of R_T and C_T with respect to the Reference plate.

Reference	$V\ [m/s]$	3.1	3.3	3.5	3.7	3.9	4.1	4.3	4.5
	Rn	4.0710^6	4.3310^6	4.5910^6	4.8610^6	5.1310^6	5.4010^6	5.6610^6	5.9210^6
	$R_T\ [N]$	33.13	37.60	42.56	46.44	51.37	56.71	62.03	68.00
	C_T	3.93110^{-3}	3.93510^{-3}	3.95510^{-3}	3.85310^{-3}	3.82610^{-3}	3.81810^{-3}	3.79510^{-3}	3.80310^{-3}
Distributed	ΔR_T%	6.03	5.52	4.14	6.00	7.48	5.74	5.70	7.25
	ΔC_T %	4.38	3.91	2.63	4.35	6.32	4.59	4.30	6.51
Midlenght	ΔR_T%	3.19	4.10	0.83	2.75	3.27	2.73	2.95	2.49
	ΔC_T %	3.26	4.12	0.78	2.77	3.44	2.99	3.12	2.66
Upstream	ΔR_T%	−0.50	−0.72	0.08	−0.96	−0.80	−1.28	−1.07	−0.41
	ΔC_T %	−1.32	−1.55	−0.66	−1.74	−1.41	−1.68	−1.84	−1.22
Downstream	ΔR_T%	0.86	0.03	−1.88	0.31	0.47	−0.35	−0.26	−0.54
	ΔC_T %	0.04	−0.72	−2.57	−0.56	−0.23	−1.12	−0.97	−1.06

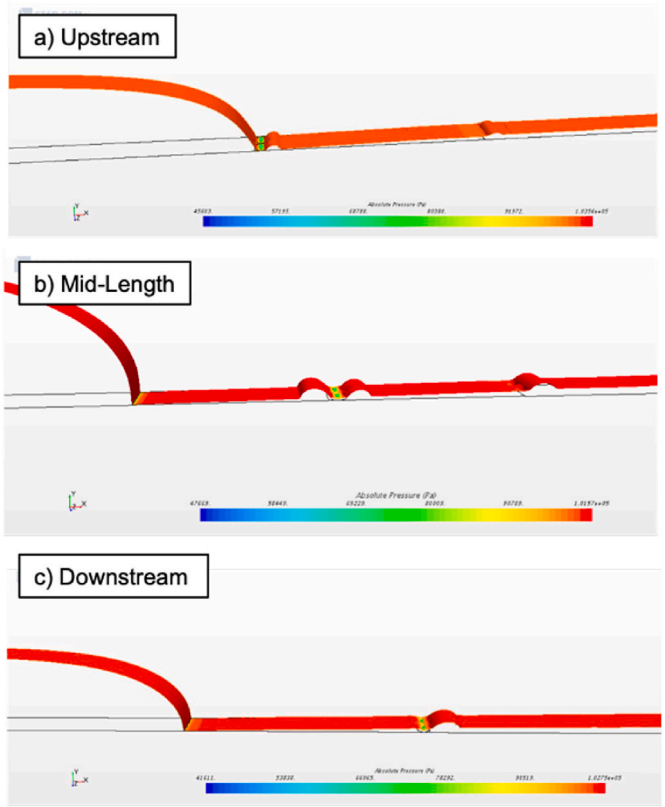

Fig. 11. Boundary layer distribution, Marino et al. (2019).

At 3.9 m/s, it shows its largest increment of drag, 7.48%. On the other hand, one can appreciate the benefits of the Upstream and Downstream configurations in drag and resistance coefficient.

Tubercles Upstream and Downstream provide a drag reduction also appreciable in the C_T curve. This benefit is shown at high Reynolds numbers, velocities higher than 3.7 m/s. Also, the Downstream configuration shows similar results at high Reynolds number. The best effect for the Upstream configuration is reported at 4.3 m/s, C_T reduction of 1.84%. Whereas for the Distributed configuration, the drag measured at the same speed is 5.70% greater than the bare flat plate.

The biomimetic tubercles create vortical structures which manipulate the flow around the bodies. The leading-edge tubercles impose a downward deflection of the flow over the upper edge of the tubercles and an upward deflection in the troughs. Thus, the presence of tubercles upstream of the flat plate may act as leading-edge tubercles on wing profiles, delaying flow separation toward the trailing edge downstream. The underlying reasons for drag reduction in the upstream and downstream configurations on a flat plate could be further exploited by conducting CFD simulations.

As the tubercles alter the shape of the flat plate, the new boundary layer further alters the virtual shape and length of the plate. Furthermore, the tubercles increase the flow interaction with the flat plate resulting in a drag increase compared to the bare flat plate. While the effect of the upstream and downstream tubercles affects the viscous pressure drag in a positive way, the mid-length configuration does not support this benefit. Similarly, the distributed configuration, which also counts more tubercles than all the others, is believed to cause increased eddy-making resistance. In other words, the disturbed streamline flow caused by the distributed tubercles results in an increased eddy-making resistance and hence increased total drag.

Fig. 11 shows the boundary layer characteristics along the flat plate in the Upstream, Mid-length and Downstream configuration. As it can be noted, the presence of biomimetic tubercles on the flat plate affects the pressure distribution and hence the boundary layer. For the Mid-length scenario, the tubercles produce a consistent pressure increase both Upstream and Downstream of their location, and the pressure distribution at the trailing edge of the flat plate seems to be affected too. The row of tubercles act as a source causing a pressure increase on the plate. The change in pressure distribution might be the cause of the positive effect on the total drag for the upstream and downstream configurations. On the other hand, the Mid-length configuration has a greater impact on the pressure distribution than the Upstream and Downstream ones, resulting

Table 4
Uncertainty Analysis of CT at the lowest and highest speed of the range.

		Lowest speed			Highest speed		
		Bias	Precision	Uncertainty	Bias	Precision	Uncertainty
Reference	%	$3.21{\cdot}10^{-5}$	$3.37{\cdot}10^{-5}$	$4.66{\cdot}10^{-5}$	$1.93{\cdot}10^{-5}$	$5.35{\cdot}10^{-5}$	$2.00{\cdot}10^{-5}$
		0.74	0.77	1.06	0.50	0.14	0.53
Distributed	%	$3.35{\cdot}10^{-5}$	$1.38{\cdot}10^{-5}$	$3.62{\cdot}10^{-5}$	$2.07{\cdot}10^{-5}$	$4.53{\cdot}10^{-5}$	$2.11{\cdot}10^{-5}$
		0.72	0.30	0.77	0.51	0.11	0.52
Mid-length	%	$3.30{\cdot}10^{-5}$	$2.54{\cdot}10^{-5}$	$4.16{\cdot}10^{-5}$	$1.97{\cdot}10^{-5}$	$5.07{\cdot}10^{-5}$	$2.04{\cdot}10^{-5}$
		0.72	0.56	0.91	0.51	0.13	0.52
Upstream	%	$3.43{\cdot}10^{-5}$	$5.32{\cdot}10^{-5}$	$6.32{\cdot}10^{-5}$	$1.92{\cdot}10^{-5}$	$1.29{\cdot}10^{-5}$	$2.31{\cdot}10^{-5}$
		0.70	1.07	1.28	0.39	0.26	0.47
Downstream	%	$3.27{\cdot}10^{-5}$	$5.22{\cdot}10^{-5}$	$6.16{\cdot}10^{-5}$	$1.93{\cdot}10^{-5}$	$3.03{\cdot}10^{-5}$	$3.60{\cdot}10^{-5}$
		0.73	1.16	1.36	0.51	0.79	0.54

in an increased total drag.

3.2. Uncertainty analysis

The uncertainty analysis followed the (ITTC, 2002) and (Coleman and Steele, 1999) procedures, as explained in the Methodology section. Below are presented the results for towing test of the tubercles configurations.

According to Table 4, the maximum uncertainty of C_T for the Upstream configuration ranges between ±1.36% at the lowest speed and between ±0.54% at the highest speed. The drag reduction of the tubercles in the Upstream configuration is 1.2% at the highest speed, confirming that the reduction observed is appreciable despite the uncertainty. Overall, the drag coefficients' uncertainty levels were considered acceptable compared to other experiments given in the literature Schultz (2002).

Further verification has been conducted comparing the CFD analysis of Marino et al. (2019) and the present experiments. Good agreement was found at $Rn \approx 5.0{\cdot}10^{6}$ for the frictional coefficients for all of the tubercled configurations tested ($C_F \approx 3.0 - 3.25{\cdot}10^{-3}$). The range of Reynolds numbers used in the CFD analysis of Marino et al. (2019) was $Rn \approx 5.0{\cdot}10^{6} - 1.5{\cdot}10^{7}$, hence greater than in the present experiment. Therefore, no complete comparison between the present results and those of Marino et al. (2019) is reported in the present manuscript.

4. Conclusions

This paper showed an experimental investigation into the effect of biomimetic tubercles on the drag of a flat plate. Four different configurations of tubercles were tested, and their total resistance coefficients were compared.

The effect of the Upstream and Downstream configurations is a drag reduction at higher Reynolds numbers. For these setups, the experiments revealed an appreciable lower resistance than the bare flat plate of 1.3% and 0.5%, respectively. The total resistance coefficients trend suggested that those reductions would grow at a higher Reynolds number. Although the advantage of head tubercles as drag reduction solution is not confirmed, their presence on specific parts of ship hulls could be justified to manipulate the flow from a biofouling management perspective.

For the Distributed and Mid-length configurations, maximum drag increases of 7.5% and 3.3% were registered. The application of such Distributed and Mid-length arrangements could be further investigated in future studies. Despite the slight drag increase, these configurations could be justified to obtain a conveniently manipulated boundary layer and flow over the plate.

The uncertainty analysis of the drag coefficients was conducted for all of the experiments. For the total resistance coefficients, an uncertainty of ±0.5% was calculated for the highest speed tested. The results of this analysis are in line with other studies confirming the repeatability of the experiments.

Different Fr numbers and Re numbers affect the drag reduction effect of the Upstream and Downstream biomimetic tubercles. The results showed that at the higher speeds of the range ($4.1 - 4.5\ m/s$) the row of tubercles positively influence the total drag of the flat plate. This positive influence might be due to the fully turbulent regime which is reached at those speeds. On the other hand, the transitory regime at lower speed is such that the oscillations in the total drag measured results in both smaller and grater drag values than the bare flat plate.

The authors appreciate that in order to give the readers a clearer picture for the application of tubercles in real life scenarios, further experimental and numerical studies may be conducted. The present manuscript intends to facilitate new research to fill the literature gap on the potentials of biomimetic tubercles.

Further experimental or numerical studies could exploit the effect of different scales, numbers, and configurations of biomimetic tubercles. Novel experimental studies might test different tubercles configurations and their effect on the resistance components. New models for CFD studies could be developed to predict the full-scale effect on ships. New models for CFD studies could be developed to predict the full-scale effect on ships. The models described in this paper can be easily variegated and eventually upgraded to more sophisticated arrangements. Different shapes, dimensions, and positions of the biomimetic tubercles on the plate could be studied.

CRediT authorship contribution statement

Roberto Ravenna: Conceptualization, Methodology, Formal analysis, Investigation, Data curation, Comparison, Writing – original draft, Visualization. **Alessandro Marino:** Conceptualization, Methodology, Comparison, Writing – review & editing. **Soonseok Song:** Data curation, Investigation, Formal analysis, Writing – review & editing. **Mehmet Atlar:** Supervision, Resources. **Osman Turan:** Resources. **Sandy Day:** Resources. **Yigit Kemal Demirel:** Conceptualization, Methodology, Supervision, Funding acquisition, Writing – review & editing, Project administration.

Declaration of competing interest

The authors declare that they have no known competing financial interests or personal relationships that could have appeared to influence the work reported in this paper.

Acknowledgement

This paper is based on the study presented at the AMT'19 Conference, which was held on 9–11 October 2019 in Rome, Italy. No specific grants were received from funding agencies in the public, commercial, or not-for-profit sectors. The authors would like to give special thanks to the staff of Kelvin Hydrodynamics Laboratory of the University of Strathclyde.

References

Bolzon, M.D., Kelso, R.M., Arjomandi, M., 2016. Tubercles and their applications. J. Aero. Eng. 29, 04015013 https://doi.org/10.1061/(ASCE)AS.1943-5525.0000491.

Bugatti Dimple Airscoop, 2020 [WWW Document], URL. https://www.bugatti.com/media/news/2020/bugatti-dimple-airscoop/.

Clapham, P.J., 2018. Humpback whale: megaptera novaeangliae. Encycl. Mar. Mamm. 489–492. https://doi.org/10.1016/B978-0-12-804327-1.00154-0.

Clapham, P.J., Mead, J.G., 1999. Megaptera Novaeangliae, 3, pp. 1–9. https://doi.org/10.2307/3504352/2600761.

Coleman, H.W., Steele, W.G., 1999. Experimentation, Validation, and Uncertainty Analysis for Engineers.

Demirel, Y.K., Uzun, D., Zhang, Y., Fang, H.-C., Day, A.H., Turan, O., 2017. Effect of barnacle fouling on ship resistance and powering. Biofouling 33, 819–834. https://doi.org/10.1080/08927014.2017.1373279.

Dobre, A., Hangan, H., Vickery, B.J., 2006. Wake control based on spanwise sinusoidal perturbations. AIAA J. 44, 485–492. https://doi.org/10.2514/1.15155.

Fish, F.E., 2009. Biomimetics: determining engineering opportunities from nature. In: Martin-Palma, R.J., Lakhtakia, A. (Eds.), International Society for Optics and Photonics, 740109. https://doi.org/10.1117/12.824106.

Fish, F.E., Lauder, G.V., 2006. Passive and active flow control by swimming fishes and mammals. Annu. Rev. Fluid Mech. 38, 193–224. https://doi.org/10.1146/annurev.fluid.38.050304.092201.

Fish, F.E., Weber, P.W., Murray, M.M., Howle, L.E., 2011. The tubercles on humpback whales' flippers: application of bio-inspired technology. Integr. Comp. Biol. 51, 203–213. https://doi.org/10.1093/icb/icr016.

Gruber, T., Murray, M.M., Fredriksson, D.W., 2011. Effect of humpback whale inspired tubercles on marine tidal turbine blades. In: Biomedical and Biotechnology Engineering; Nanoengineering for Medicine and Biology, vol. 2. ASME, pp. 851–857. https://doi.org/10.1115/IMECE2011-65436.

Hasheminejad, S.M., Mitsudharmadi, H., Winoto, S.H., Winoto, Sonny Handojo, 2013. Effect of flat plate leading edge pattern on structure of streamwise vortices generated in its boundary layer. Artic. J. Flow Control 2, 18–23. https://doi.org/10.4236/jfcmv.2014.21004.

IMO, 2015. Third IMO GHG Study 2014 Executive Summary and Final Report.

ITTC, 2017a. Final Report and Recommendations to the 28th ITTC.

ITTC, 2017b. ITTC-recommended Procedures and Guidelines Uncertainty Analysis, Instrument Cali-Bration ITTC Quality System Manual Recommended Procedures and Guidelines Procedure.

ITTC, 2011. ITTC-recommended Procedures and Guidelines.

ITTC, 2002. ITTC uncertainty analysis, example for resistance test. ITTC Recommended Procedures and Guidelines, Procedure 7, 5-02-02-02, Revision 01.

Lewis, E.V., 1988. Principles of Naval Architecture, Second Rev. The Society of Naval Architects and Marine Engineers.

Marino, A., Atlar, M., Demirel, Y.K., 2019. An investigation of the effect of biomimetic tubercles on a flat plate. In: ASME 2019 38th International Conference on Ocean, Offshore and Arctic Engineering. OMAE, 2019.

Mercado, E., 2014. Short note: tubercles: what sense is there? Aquat. Mammalia 40, 95–103. https://doi.org/10.1578/AM.40.1.2014.95.

Miklosovic, D.S., Murray, M.M., Howle, L.E., Fish, F.E., 2004. Leading-edge tubercles delay stall on humpback whale "Megaptera novaeangliae… flippers. Phys. Fluids 16. https://doi.org/10.1063/1.1688341.

Mohseni, K., Mittal, R., Fish, F., 2006. Special issue featuring selected papers from the mini-symposium on biomimetic & bio-inspired propulsion (boulder, CO, USA, 26 June 2006). Bioinspiration Biomimetics 1 (4). https://doi.org/10.1088/1748-3190/1/4/E01.

Schultz, M.P., 2002. The relationship between frictional resistance and roughness for surfaces smoothed by sanding. J. Fluid Eng. 124, 492. https://doi.org/10.1115/1.1459073.

Shi, W., Atlar, M., Norman, R., Aktas, B., Turkmen, S., 2016a. Numerical optimization and experimental validation for a tidal turbine blade with leading-edge tubercles. Renew. Energy 96, 42–55.

Shi, W., Atlar, M., Norman, R., Aktas, B., Turkmen, S., 2015. Biomimetic Improvement for a Tidal Turbine Blade.

Shi, W., Atlar, M., Rosli, R., Aktas, B., Norman, R., 2016b. Cavitation observations and noise measurements of horizontal axis tidal turbines with biomimetic blade leading-edge designs. Ocean Eng. 121, 143–155. https://doi.org/10.1016/J.OCEANENG.2016.05.030.

Song, S., Dai, S., Demirel, Y.K., Atlar, M., Day, S., Turan, O., 2021. Experimental and theoretical study of the effect of hull roughness on ship resistance. J. Ship Res. 65, 62–71. https://doi.org/10.5957/josr.07190040.

Taubes, G., 2000. Biologists and engineers create a new generation of robots that imitate life. science.sciencemag.org.

Vincent, J.F.V., Bogatyreva, O.A., Bogatyrev, N.R., Bowyer, A., Pahl, A.-K., 2006. Biomimetics: its practice and theory. J. R. Soc. Interface 3, 471. https://doi.org/10.1098/RSIF.2006.0127.

Weber, P.W., Howle, L.E., Murray, M.M., Fish, F.E., 2009. Lift and drag performance of odontocete cetacean flippers. J. Exp. Biol. 212, 2149–2158. https://doi.org/10.1242/jeb.029868.